Mechanical performance of carbon-glass hybrid composite joints in quasi-static tension and tension-tension fatigue

Umair Javaid[1], Chen Ling[1,2] and Philip Cardiff[1]

[1]School of Mechanical and Materials Engineering, University College Dublin, Ireland

[2]Department of Mechanical Engineering, Aalto University, Finland

June 8, 2020

Abstract

The ever increasing size of wind turbines has given rise to a need for robust glass to carbon joint designs. This study investigates the effect of different ply layups on the static and fatigue behaviour of hybrid glass/carbon fibre composite joints. Uni-directional carbon fibre prepreg was co-cured to 8H glass prepreg using an overlap to thickness ratio of 20:1, where four joint designs were examined: scarf, interleaving and two forms of double scarf. The joints were tested statically in uniaxial tension and dynamically in tension-tension fatigue. Finite element analysis has been performed to provide insight into stress distributions within each joint. The double scarf joint (with glass on the outside) was found to perform best in fatigue and static tension, while the interleaving joint performed second best in fatigue in static tension but poorest in fatigue. For joint designs that will be used under highly stressed cyclic loading conditions, the current study indicates that static tests alone are a poor

indicator of the joint performance and fatigue tests are required.

Keywords

Hybrid composite joint; Carbon fibre; Glass fibre; Tension-tension fatigue; Finite element analysis

1 Introduction

In wind turbine design, as the blade length increases, the specific length and stiffness also needs to increase [1–3]. This problem can be addressed by replacing commonly used glass fibre (GF) with carbon fibre (CF). CF is stiffer, stronger, more fatigue-resistant and less dense but comes at a considerably higher cost [4, 5]. Consequently, the hybridisation of GF with CF has received significant attention where CF and GF are combined in a single structure, with CF placed in critical regions [6–14].

Efficient joining of different fibre types is a challenge due to their anisotropy, low strain to failure and difference in thermal expansion, all resulting in large residual thermal stresses [15, 16]. Adhesive bonding is a promising approach for creating such hybrid composite joints, where several joint designs are possible [17]. A significant challenge, however, is that the strength in the joint region is less than that of the the virgin laminate. This is due to discontinuous fibres in the interface region and stress concentrations in the adhesive and laminate layers [18]. Hence, it is essential to investigate the reliability of interfacial joints subjected to representative loading types [18]. Of particular interest is the fatigue response of such composite structures which are frequently exposed to repeated cyclic loads, during which concentrations at the ply drop-offs can cause premature failure. The fatigue life of aerodyanamic structures is heavily

dependent on regions of stress concentration. Micro-cracking in such regions can lead to catastrophic failure of the entire structure in a relatively short number of cycles. As such, it is important to find a suitable CF-GF hybrid joint design so that stresses remain well below the endurance limits of the material [19]. The current article aims to build on the significant progress in the design of hybrid joints, e.g. [6], where focus is given to the improving the understanding of the fatigue performance of these adhesive joints.

The remainder of this article is structured as follows: Section 2 describes the design and fabrication of the four hybrid joints, the materials, and the testing methods. In addition, the finite element model setup is outlined. In Section 3, the experimented and numerical results are presented. Finally, the article concludes in Section 4 by summarising the main results and their implications.

2 Methods

2.1 Hybrid joint design

Four hybrid CF-GF joint designs are selected to quantify the effect of joint geometry on the static and dynamic capacity (Figure 1): interleaving, scarf, double scarf-I (carbon on the outside) and double scarf-II (glass on the outside). Each joint design has an overlap region of length 80 mm and a thickness-to-length ratio of 1:20.

The joints are produced as follows:

- Interleaving: successive ply terminations are offset in opposing directions along the length of the joint while retaining symmetry about mid-plane;
- Scarf: linearly increasing the the CF ply length from the top to the bottom of the joint, while decreasing the corresponding GF ply length;

- Double scarf-I: linearly decreasing the CF ply length from the top to the middle of the joint, and then linearly increasing the CF ply length from the middle to the bottom of the joint. The GF ply lengths are correspondingly increased and decreased;

- Double scarf-II: similar to the double scarf-I joint, however, with the length of the GF plys linearly decreasing from the top to the middle and then linearly increasing again to the bottom.

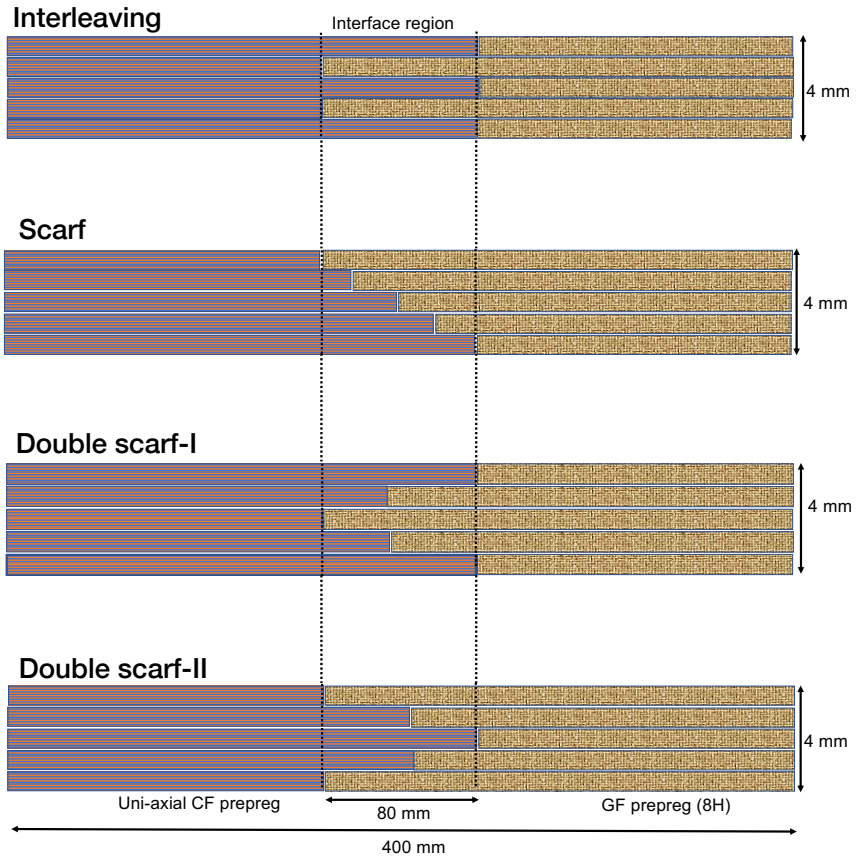

Figure 1: Hybrid CF-GF joint designs

2.2 Materials

The hybrid laminates were fabricated by combining M21/37%/7581 GF reinforced prepregs from Hexcel with XC130 CF reinforced prepregs from Easy Composites. Both prepregs systems have similar cure temperatures and were found to be compatible for co-curing. Material data for both prepregs is given in Table 1.

Table 1: Material data

Material	Units	GF prepreg	CF prepreg
Weave count	/tow	8 harness strain	12 K
Fibre density	g/m^2	2.56	1.79
Resin density	g/m^2	1.28	1.3
Cured ply thickness	mm	0.26	0.13
Nominal fibre volume	%	46	57.42
Nominal tensile strength	MPa	444	2,207
Nominal tensile modulus	GPa	25.5	141

2.3 Sample preparation

A hand lay-up technique was employed to fabricate the hybrid CF-GF joints. Unidirectional CF and 8H GF prepregs were laid on top of a flat aluminium plate according to the design required. The stacking sequence and ply lengths are given in Table 2. The joints were prepared in such a way that fifteen layers of CF prepreg were stacked together with fifteen layers of GF prepreg keeping a constant overlap joint length of 80 mm. The laminates were cured using a vacuum-supported hot-press. During curing, a constant air pressure of 0.2 MPa was applied and a trapezoidal temperature profile was followed:

1. The temperature is linearly increased from room temperature to 180°C over a duration of 2 hours;

2. The temperature is held at 180°C for 2 hours;

3. The temperature is then allowed to cool to room temperature over night.

Further details of the in-house lay up and curing are given in Appendix A.

Once cured, a diamond cutting wheel was used to cut the specimens into rectangular strips with dimensions of 200 mm × 25 mm. In advance of testing, aluminium end tabs with a thickness of 2 mm were bonded to the specimen using toughened cyanoacrylate adhesive glue. These end tabs help avoid premature failure in the grip region.

Table 2: Lay up sequence of laminates (mm)

Ply number	Interleaving		Scarf		Double Scarf-I		Double Scarf-II	
	CF	GF	CF	GF	CF	GF	CF	GF
1	240	160	240	160	240	160	160	240
2	240	160	240	160	240	160	160	240
3	240	160	240	160	240	160	160	240
4	160	240	220	180	220	180	180	220
5	160	240	220	180	220	180	180	220
6	160	240	220	180	220	180	180	220
7	240	160	200	200	200	200	200	200
8	240	160	200	200	200	200	200	200
9	240	160	200	200	200	200	200	200
10	160	240	180	220	220	180	180	220
11	160	240	180	220	220	180	180	220
12	160	240	180	220	220	180	180	220
13	240	160	160	240	240	160	160	240
14	240	160	160	240	240	160	160	240
15	240	160	160	240	240	160	160	240

2.4 Quasi-static tensile testing method

Quasi-static uniaxial tensile testing was performed on the hybrid joints according to the ISO-527 standard [20]. An Instron 8501 universal testing machine was used, with hydraulic wedge-type grips and a 250 kN capacity load cell. The strip specimens (200 mm × 25 mm) were loaded in displacement control with a cross head speed of 2 mm/min and were tested to failure. For each joint design,

four repeats were performed and the failure load was recorded. Subsequently, the failure patterns of the fractured samples were analysed using an optical microscope.

2.5 Dynamic tension-tension fatigue testing method

Dynamic tension-tension fatigue tests were performed in accordance with the ASTM D3479 standard [21]. The pristine specimens were fatigue tested at four different stress levels: 60%, 70%, 80% and 90% of the Effective Failure Load (EFL) value. The EFL is calculated as the mean failure load from the quasi-static tension tests minus one standard deviation. Testing was conducted under load control by applying a sinusoidal load about the mean load at a frequency of 5 Hz and stress ratio of 0.1 (Figure 2). Four repeats were performed for each joint at each load level, and the number of cycles to failure was recorded.

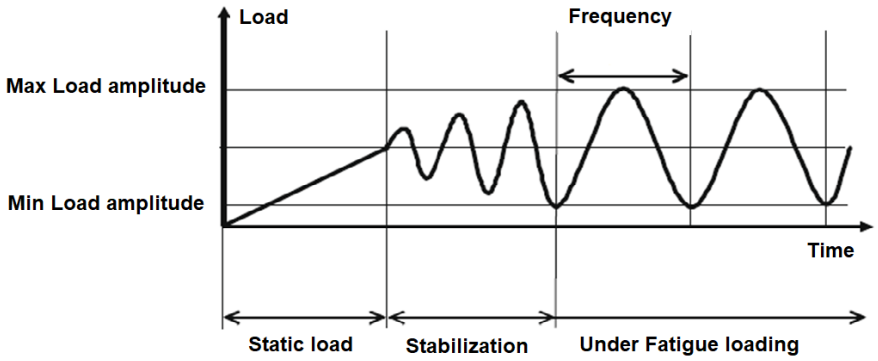

Figure 2: Fatigue loading scheme (figure taken from [22])

2.6 Finite element analysis

To provide insight into the stress distributions within the four joint designs, finite element analysis of the joints in tension has been performed using commercial software Abaqus (version 6.14). The models assume 2-D plane strain

conditions and neglected inertia and gravity. The specimen geometry between the grips was taken as the solution domain. For the GF, the Young's modulus was taken as 25.5 GPa and the Poisson's ratio as 0.2; whereas for the CF, the Young's modulus was taken as 141 GPa and the Poisson's ratio as 0.2. These mechanical properties were determined from uniaxial tensile tests performed on both the GF and CF. The models were meshed using 8-node bi-quadratic uniform structured quadrilaterals with reduced integration (Abaqus element code CPE8R). Following a mesh sensitivity analysis (detailed given in Appendix B), an element size of 0.125 mm was selected; the 1 mm mesh is shown in Figure 3. To compare the relative stress distributions within the joint designs, a constant negative pressure of 0.75 MPa was applied to one end of the joint, and a zero displacement condition was applied to the opposite end.

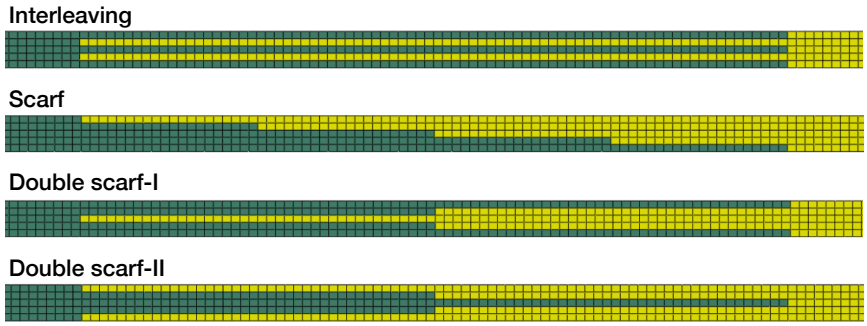

Figure 3: Close-up of the 1 mm element size finite element meshes and material distributions (CF in green, GF in yellow) within the overlap region for the four joint designs

3 Results and discussion

3.1 Quasi-static tensile testing results

Figure 4 depicts a typical stress vs strain curve for each joint design. The stress has been calculated by dividing the load by the cross sectional area of the GF

region. It is found that the force trace for each joint is characterised by an initial nominally linear elastic region followed by a brittle failure. A summary of the

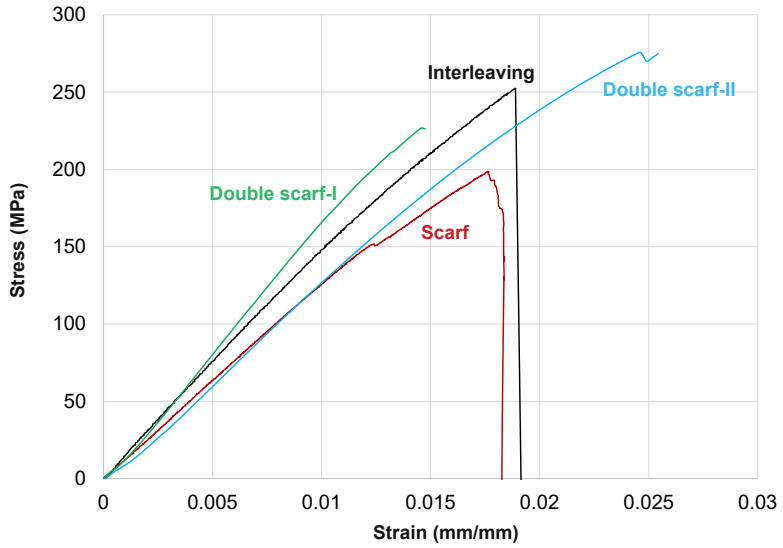

Figure 4: Representative stress vs strain graph for the four hybrid joint designs

mean strength for each joint design is given in Table 3 and Figure 5. In order of improving performance, the mean strength varied from 208.48±5.35 MPa in the scarf design, 209.93±14.62 MPa in the double scarf-I, 252.35±9.75 MPa in the interleaving, to 281.40±6.58 MPa in the double scarf-II.

Table 3: Summary of the tensile testing strength results

Joint design	Mean strength & standard deviation (in MPa)
Interleaving	252.35±9.75
Scarf	208.48±5.35
Double scarf-I	209.93±14.62
Double scarf-II	281.40±6.58

Side-profile images of the fractured samples from the quasi-static tensile tests (left column of images in Figure 6) reveal the fracture pattern for each joint design. The interleaving joint fails via a perpendicular fracture at the

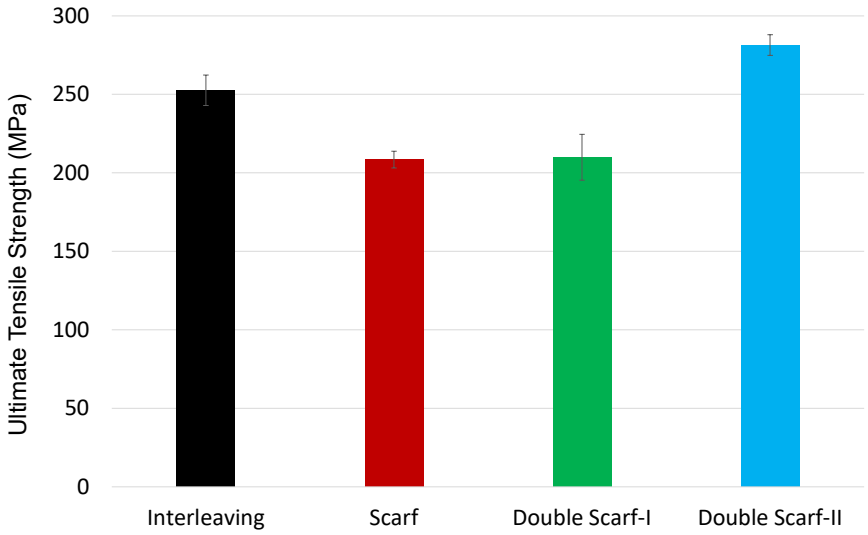

Figure 5: Ultimate strength of different laminates

GF end of the overlap region, resulting in matrix cracking, fibre breakage and delamination of plys. In contrast, the scarf joint failed by delaminating along the GF-CF bond, hence the relatively low failure strength. For the double scarf-I design, a perpendicular crack initiated in the GF within the centre of the overlap region; this crack then propagates perpendicularly to the CF interface and ends with an interface delamination-type failure. Finally, for the double scarf-II design, a perpendicular fracture occurs at the GF end of the overlap region, similar to the interleaving design. It can be seen that the best performing joints in quasi-static tension (interleaving and double scarf-II) failed at the GF end of the overlap region, unlike the scarf and double scarf-I designs which failed within the body of the overlap region.

To understand the observed behaviour, it is important to recognise that the CF used in the current study has a nominal strength that is five times greater than that of the GF (Table 1). Consequently, as the CF and GF had approximately the same thickness, it would be expected that the failure would

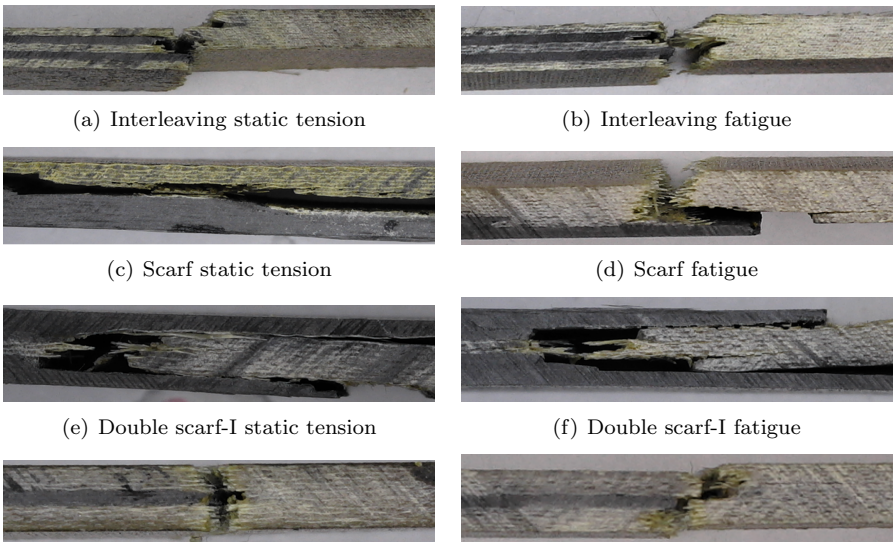

(a) Interleaving static tension (b) Interleaving fatigue

(c) Scarf static tension (d) Scarf fatigue

(e) Double scarf-I static tension (f) Double scarf-I fatigue

(g) Double scarf-II static tension (h) Double scarf-II fatigue

Figure 6: Typical fracture patterns for quasi-static tension and tension-tension fatigue (60% EFL). For the fatigued samples, the same fracture pattern was observed at all EFL values.

initiate in the GF. This was observed in three of the joint designs (interleaving, double scarf-I and double scarf-II). In the case of the interleaving and double scarf-II (GF outside), a transverse fracture is seen to occur at the GF end of the joint (Figure 6). For the double scarf-I joint (CF outside), the GF fails near the centre of the joint where the GF is thinner, and hence the stress is higher. The only joint that did not fail in the GF was the scarf joint where interfacial failure occur in the joint itself; this explains the relatively low value of strength, which is compounded by the asymmetric (eccentric) stiffness of the joint [6]. Comparing the measured strengths to similar joints in literature, Ahamed et al. [6] reported tensile strengths for a variety of interleaving joints in the range of 278 to 354 MPa, in comparison to 208 to 281 MPa in the current study; the reason for differences can be primarily attributed to the use of unidirectional GF in the Ahamed et al. [6] study, in contrast to the lower strength 8H GF used

here. It has also been noted that increasing the overlap length has the potential to increase the joint strength [6].

3.2 Dynamic tension-tension fatigue testing results

The mean number of cycles to failure of all joint designs, at four different stress levels (60%, 70%, 80% and 90% of the EFL), are shown in Figure 7. This same information is presented in the standard S-N curve format in Figure 8, and results for all repeats are given in Appendix C. The S-N response follows a similar trend for all joint designs: at the greatest stress amplitudes, the number of cycles to failure are lowest; as the stress amplitude is reduced, the number of cycles to failure increases, and when plotted in the typical linear-log fashion, the trend follows an approximately straight line. Considering the scarf, double scarf-I and double scarf-II joints, the double scarf-I (GF on outside) performs best at the three higher stress amplitudes (70%, 80% and 90%) followed by the double scarf-II design (CF on outside), and then the scarf. Somewhat surprisingly the trend changes for the double scarf-I joint at the lowest stress amplitude level (60%), where it is outperformed by the double scarf-II design and marginally by the scarf design. At the higher stress amplitudes, the scarf design performs the poorest by far, failing in fives times less cycles than the double scarf-I joint at 90% EFL. In contrast to the other three, the interleaving design shows a steeper trend at the higher stress amplitudes: the number of cycles to failure at 80% EFL is only 15% greater than at 90% EFL, in contrast to the double scarf-I joint where 306% more cycles are required going from 90% to 80% EFL. At the lower stress amplitudes (60% and 70%), the trends recovers to be closer to the other joint designs, but the number of cycles to failure at 60% EFL is lowest for the interleaving design, 15,821 cycles vs 68,711 for the double scarf-II design (best performer at 60% EFL).

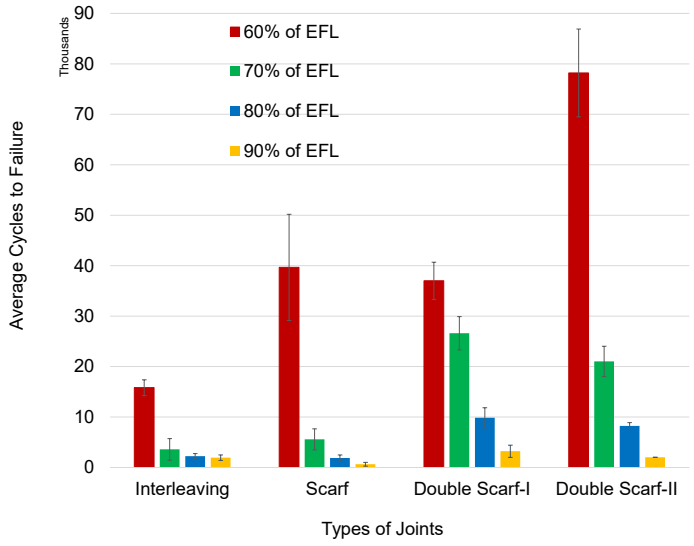

Figure 7: Tension-tension fatigue results: mean number of cycles to failure for four stress-ratio levels with error bars indicating the standard deviation

Examining next the typical failure modes seen in fatigue (right column in Figure 6 for 60% EFL), the interleaving, double scarf-I and double scarf-II joints all failed in a similar manner in both quasi-static tension and fatigue, with matrix cracking, fibre breakage and delamination of plys. The one exception was the scarf joint, which failed failed via a perpendicular crack near the GF end of the overlap in fatigue, which is in contrast to the interfacial failure of the GF-CF bond in quasi-static tension. The fracture patterns shown in Figure 6 (right column) correspond to 60% EFL, however, the same failure pattern was observed at all tested EFL values.

From these results, we can see that that two best performing designs in fatigue are the double scarf-I (CF on outside) and double scarf-II (GF on outside). As the fatigue EFL is calculated based on the quasi-static strength results for each design, the double scarf-II (GF on outside) endured absolute values of stress in fatigue that were over 30% greater than those experienced by the double scarf-I (CF on outside) joint. In this way, if absolute strength and fatigue

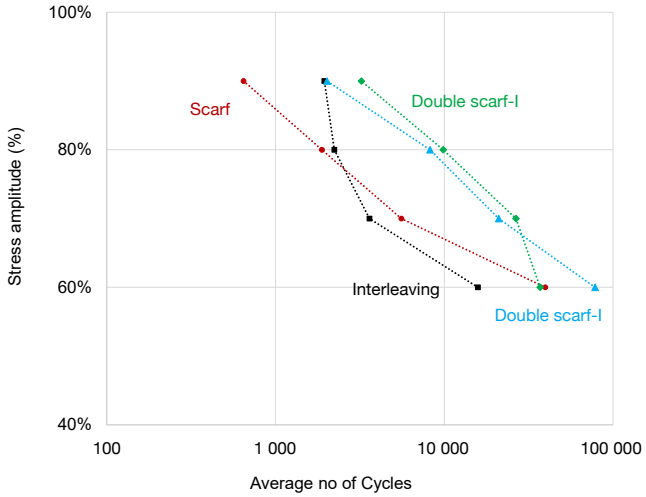

Figure 8: S-N curve of all joint designs. The reported number of cycles is the average of four repeats.

performance are desired, the double scarf-II (GF on outside) is the clear best. Conversely, although the interleaving design performed well in static tension, it was one of the two most inferior designs in fatigue. A somewhat redeeming factor is that the interleaving design endured greater absolute loads in fatigue than the scarf and double scarf-I designs, once again as the EFL is based on the static results. Finally considering the simple scarf design, it performed poor under both static and fatigue loading. A possible explanation for the poor performance of the scarf may be significant bending introduced due to the asymmetric stiffness of the design. As from the simple scarf joint, the reason why the double scarf-II (GF on outside) performs best and why the interleaving design performs much worse in fatigue than static tension is not clear; however, the ply drops tend to act as stress concentration (shown numerically in the next section) and a key concern in the joint design. When examining demonstrator CF-GF wind turbine blade joints, Pappa et al. [19] noted that even though the ply-drops absorb some fracture energy, they tend to act as a point of weakness that leads to a

transverse opening. They also stated that designing the most effective ply-drops is of paramount importance. Ply drops are not the only influencing factor which determines joint performance, with defects and anomalies having a significant influence on the fatigue life and fatigue life uncertainty [23]. Furthermore, as noted by Banea and da Silva [24], the numerous failure mechanisms means that there is a lack of reliable failure criteria composite joints.

3.3 Finite element stress results

To allow fair comparison between the joint designs, the *stress ratio* distributions for each joint are compared, where the stress ratio is defined as the ratio of the maximum principal stress to the applied average stress at the end of the joint. As failure in the physical joints was located in the GF or at the GF-CF interface, the stress distribution in the GF is the only shown in Figure 9. For the interleaving, double scarf-I and double scarf-II designs, the greatest stress concentrations occur at the drop-off of the CF plys. These stress concentration locations agree with the failure position seen in the experiments. Unlike the other three designs, the scarf has an asymmetric stiffness about its centreline resulting in a rotation of the overlap region during loading. This can be seen in the typical bending stress profile seen in the joint, with regions of tensile stress on the outer surface of the GF and compressive stresses at the GF-CF interface. As a result of this rotation, opening stresses are concentrated at the free-surface end of the GF-CF interface promoting the interfacial failure seen in the experiments.

In all cases, the location of first failure seen in the experiments occurs in regions of high stress concentration seen in the simulations. Predicting the load at which the joints fail statically and in fatigue is however not trivial. Linear analysis correctly predicts the location of initial failure, however, to predict the

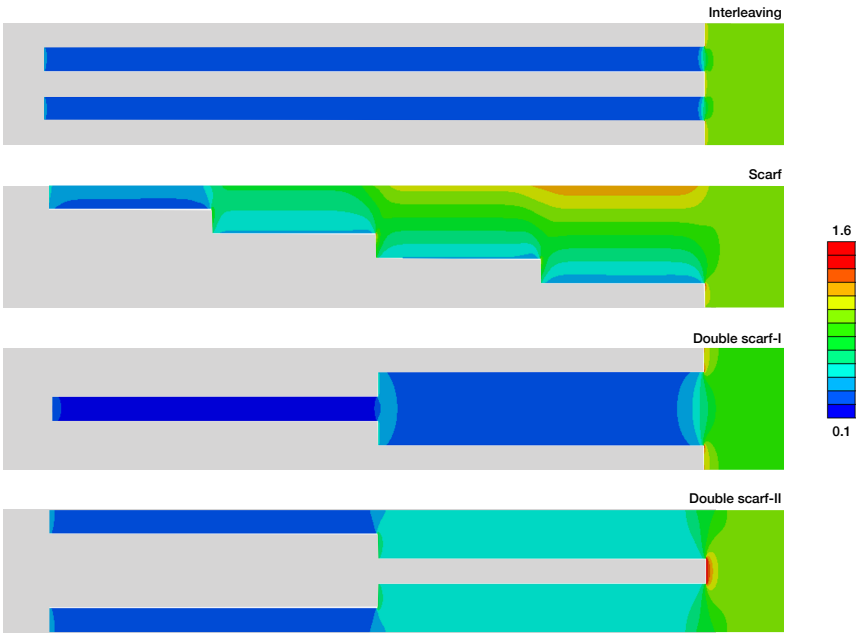

Figure 9: Glass-fibre stress ratio distributions in the four joint designs, where the stress ratio is defined as the max principal stress divided by the stress applied at the end of the joint. The geometry has been scaled by a factor of 0.2 in the horizontal direction to allow easier visualisation. The carbon-fibre is shown in grey.

load and type of failure, geometric details of the joint microstructure would need to be combined with an appropriate failure model, for example, cohesive zones or damage models. Furthermore, the predicted absolute value of maximum stress in the current analysis will not be physical due to the presence of unphysical singularities at the sharp corners [25], which could be overcome through appropriate inclusion of micro geometric details and failure models. This is outside the scope of the current article, but such an approach has been successfully applied in Ahamed et al. [10] to analyse static failure of interleaving joint designs.

4 Conclusion

In this article, four hybrid GF-CF joint designs have been tested in quasi-static uniaxial tension and tension-tension fatigue. The failure loads and modes have been measured for all joints and the following main conclusions can be drawn:

- In quasi-static tension, the double scarf-II (GF on outside) was found to be the strongest, followed by the interleaving design. The scarf and double scarf-II (CF on outside) were found to be the weakest. The failure mode for all joints, apart from the scarf, was a perpendicular fracture at the GF end of the overlap region. The scarf joint failed by delamination of the GF-CF interface.

- In tension-tension fatigue, the double scarf-II (GF on outside) and double scarf-I designs performed the best; however, as the maximum load in fatigue was based on the quasi-static failure load, the the double scarf-II performed far better in absolute terms. The interleaving and scarf designs were seen to perform the poorest, followed by the interleaving design. The scarf and double scarf-II (CF on outside) were found to be the weakest.

- Finite element analysis confirms stress concentrations located at the CF ply drop-off correctly indicating the initial failure location for all joint designs. In the case of the scarf design, the asymmetry of the joint cause rotation of the overlap region encouraging interfacial failure, as seen experimentally.

- Overall, the results indicate that the double scarf-II (glass on outside) is the best of the four designs examined for high stress-high fatigue applications, such as in tidal turbines or larger wind turbines.

5 Acknowledgements

Financial support is gratefully acknowledged from the Irish Composites Centre (IComp), as well as technical input from Adrian Doyle at ÉireComposites Teo. The authors are grateful for technical assistance from and discussions with Michael Donohue, Pierre Aumjaud, Clemence Rouge and Alojz Ivanković from University College Dublin.

6 Appendix A: Composite laminate manufacturing

Figure 10 shows a schematic of the laminate manufacturing process.

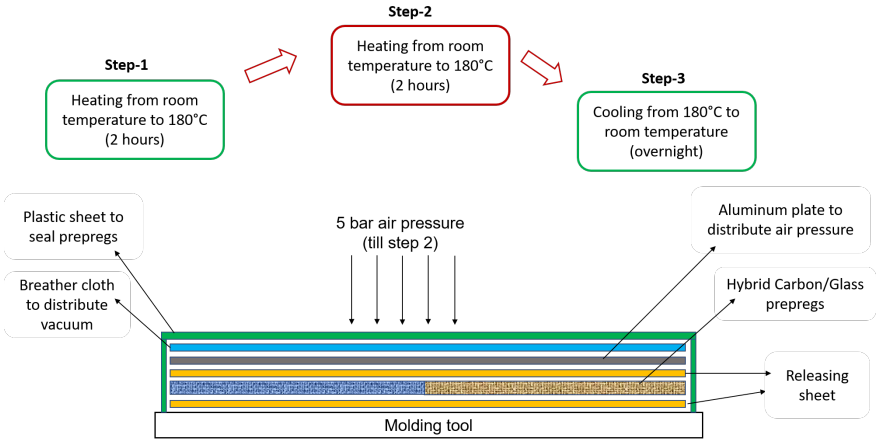

Figure 10: Schematic of laminate fabrication

7 Appendix B: Finite element mesh sensitivity analysis

For each of the four joint designs, four element sizes were analysed: 1 mm, 0.5 mm, 0.25 mm and 0.125 mm, corresponding to 1,625, 6,500, 26,000 and 104,000 elements respectively. Figure 11 shows the stress ratio distribution for the overlap region of the double scarf-II joint for four successively refined meshes. Similar trends are seen for the other three joint designs.

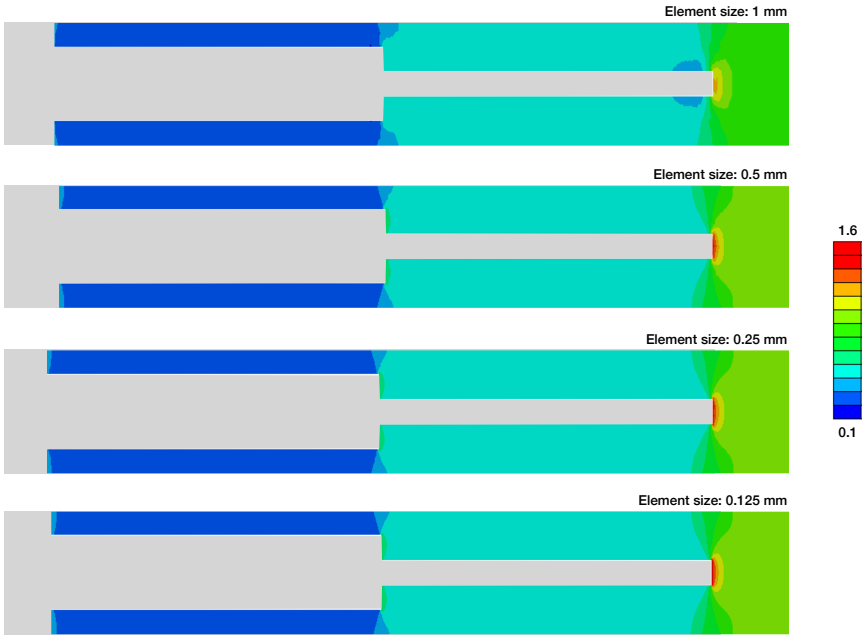

Figure 11: Distribution of stress ratio for four successively refined meshes of the double scarf-II joint design. Similar trends are seen for the other three joint designs.

8 Appendix C: Tension-tension fatigue complete results

Table 4 gives the loading amplitude for joint design as well as the number of cycles to failure for each repeat.

Table 4: Fatigue testing results

Design	Load amplitude	Estimated failure load	Load upper limit	Load lower limit	Number of cycles to failure
	%	kN	kN	kN	
Interleaving		27.00	16.20	1.62	15,821±1,574
Scarf	60	20.80	12.48	1.25	39,669±10,529
Double Scarf-I		18.27	10.96	1.10	36,995±3,702
Double Scarf-II		24.68	14.81	1.48	68,711±19,365
Interleaving		27.00	18.90	1.89	3,601±2,137
Scarf	70	20.80	14.56	1.46	5,572±2,092
Double Scarf-I		18.27	12.79	1.28	26,604±3,304
Double Scarf-II		24.68	17.28	1.73	21,027±3,002
Interleaving		27.00	21.60	2.16	2,231±533
Scarf	80	20.80	16.64	1.66	1,882±616
Double Scarf-I		18.27	14.62	1.46	9,865±1,986
Double Scarf-II		24.68	19.75	1.97	8,237±668
Interleaving		27.00	24.30	2.43	1,948±535
Scarf	90	20.80	18.72	1.87	647±379
Double Scarf-I		18.27	16.44	1.64	3,224±1,212
Double Scarf-II		24.68	22.22	2.22	2,021±30

9 Data availability

The raw data required to reproduce these findings will be available to download from a ResearchGate.com link that will be made available once the article has been published. Similarly, the processed data required to reproduce these findings are available to download from the same ResearchGate.com link. This sentence will be updated once the article has been accepted.

References

[1] M. H. Mohamed and K. K. Wetzel, "3D woven carbon/glass hybrid spar cap for wind turbine rotor blade," *Journal of Solar Energy Engineering*, vol. 128, no. 4, pp. 562–573, 2006.

[2] S.-Y. Bae and Y.-H. Kim, "Structural design and analysis of large wind turbine blade," *Modern Physics Letters B*, vol. 33, no. 14n15, p. 1940032, 2019.

[3] W. Ostachowicz, M. McGugan, J.-U. Schröder-Hinrichs, and M. Luczak, *MARE-WINT: new materials and reliability in offshore wind turbine technology*. Springer, 2016.

[4] L. Hamill, D. C. Hofmann, and S. Nutt, "Galvanic corrosion and mechanical behavior of fiber metal laminates of metallic glass and carbon fiber composites," *Advanced Engineering Materials*, vol. 20, no. 2, p. 1700711, 2018.

[5] A. Lefeuvre, S. Garnier, L. Jacquemin, B. Pillain, and G. Sonnemann, "Anticipating in-use stocks of carbon fibre reinforced polymers and related waste generated by the wind power sector until 2050," *Resources, Conservation and Recycling*, vol. 141, pp. 30 – 39, 2019.

[6] J. Ahamed, M. Joosten, P. Callus, M. R. Wisnom, and C. H. Wang, "Ply-overlap hybrid technique for joining dissimilar composite materials," *Materials & Design*, vol. 100, pp. 157 – 167, 2016.

[7] L. Thomas and M. Ramachandra, "Advanced materials for wind turbine blade-a review," *Materials Today: Proceedings*, vol. 5, no. 1, pp. 2635–2640, 2018.

[8] S. Fotouhi, J. Clamp, A. Bolouri, T. R. Pozegic, and M. Fotouhi, "Investigating polyethersulfone interleaved glass/carbon hybrid composite under impact and its comparison with glare," *Composite Structures*, vol. 226, p. 111268, 2019.

[9] M. Kalantari, C. Dong, and I. J. Davies, "Effect of matrix voids, fibre misalignment and thickness variation on multi-objective robust optimization of carbon/glass fibre-reinforced hybrid composites under flexural loading," *Composites Part B: Engineering*, vol. 123, pp. 136–147, 2017.

[10] J. Ahamed, M. Joosten, P. Callus, S. John, and C. H. Wang, "Ply-interleaving technique for joining hybrid carbon/glass fibre composite materials," *Composites Part A: Applied Science and Manufacturing*, vol. 84, pp. 134 – 146, 2016.

[11] A. D. Evans, L. T. Harper, T. A. Turner, and N. A. Warrior, "Joint design of continuous/discontinuous hybrid carbon fibre composites," in *21st International conference on composite materials*, 2017.

[12] M. Damghani, N. Ersoy, M. Piorkowski, and A. Murphy, "Experimental evaluation of residual tensile strength of hybrid composite aerospace materials after low velocity impact," *Composites Part B: Engineering*, vol. 179, p. 107537, 2019.

[13] C. Li, G. Xian, and H. Li, "Tension-tension fatigue performance of a large-diameter pultruded carbon/glass hybrid rod," *International Journal of Fatigue*, vol. 120, pp. 141–149, 2019.

[14] L. S. Yee and H. Ahmad, "XFEM modelling of single-lap kenaf fibre composite hybrid joints under quasi-static loading," *Plastics, Rubber and Composites*, vol. 48, no. 2, pp. 48–56, 2019.

[15] P.-y. Hung, K.-t. Lau, L.-k. Cheng, J. Leng, and D. Hui, "Impact response of hybrid carbon/glass fibre reinforced polymer composites designed for engineering applications," *Composites Part B: Engineering*, vol. 133, pp. 86–90, 2018.

[16] J. Guo, X. Gao, E. Toma, and U. Netzelmann, "Anisotropy in carbon fiber reinforced polymer (CFRP) and its effect on induction thermography," *Ndt & E International*, vol. 91, pp. 1–8, 2017.

[17] R. B. Ladani, K. Pingkarawat, A. T. Nguyen, C. H. Wang, and A. P. Mouritz, "Delamination toughening and healing performance of woven composites with hybrid z-fibre reinforcement," *Composites Part A: Applied Science and Manufacturing*, vol. 110, pp. 258–267, 2018.

[18] R. D. Adams, R. D. Adams, J. Comyn, W. C. Wake, and W. Wake, *Structural adhesive joints in engineering*. Springer Science & Business Media, 1997.

[19] E. J. Pappa, J. J. Murray, M. Walls, P. Alam, T. Flanagan, A. Doyle, S. Di Noi, E. D. McCarthy, and C. M. Ó. Brádaigh, "Fatigue life analysis of hybrid e-glass/carbon fibre powder epoxy materials for wind turbine blades," *18^{th} European Conference on Composite Materials*, 2019.

[20] I. O. for Standardization, "ISO 527-1:2019: Plastics - determination of tensile properties - part 1: General principles," 2019.

[21] A. International, "ASTM D3479/D3479M-19: Standard test method for tension-tension fatigue of polymer matrix composite materials," 2019.

[22] Z. Wu, X. Wang, K. Iwashita, T. Sasaki, and Y. Hamaguchi, "Tensile fatigue behaviour of FRP and hybrid FRP sheets," *Composites Part B: Engineering*, vol. 41, no. 5, pp. 396 – 402, 2010.

[23] J. Goh, S. Georgiadis, A. C. Orifici, and C. H. Wang, "Effect of disbonds on the fatigue endurance of composite scarf joints," in *Advanced Materials Research*, vol. 891, pp. 191–196, Trans Tech Publ, 2014.

[24] M. D. Banea and L. F. M. da Silva, "Adhesively bonded joints in composite materials: An overview," *Proceedings of the Institution of Mechanical Engineers, Part L: Journal of Materials: Design and Applications*, vol. 223, no. 1, pp. 1–18, 2009.

[25] A. Gacoin, P. Lestriez, J. Assih, A. Objois, and Y. Delmas, "Comparison between experimental and numerical study of the adhesively bonded scarf joint and double scarf joint: Influence of internal singularity created by geometry of the double scarf joint on the damage evolution," *International journal of adhesion and adhesives*, vol. 29, no. 5, pp. 572–579, 2009.